2017

Rheological Characterization of Liquid-to-Solid Transitions in Bulk Polyelectrolyte Complexes

Yalin Liu
University of Massachusetts Amherst

Brian Momani
University of Massachusetts Amherst

H. Henning Winter
University of Massachusetts Amherst

Sarah L. Perry
University of Massachusetts Amherst

Recommended Citation
Liu, Yalin; Momani, Brian; Winter, H. Henning; and Perry, Sarah L., "Rheological Characterization of Liquid-to-Solid Transitions in Bulk Polyelectrolyte Complexes" (2017). *Soft Matter*. 847.
https://doi.org/10.1039/C7SM01285C

Soft Matter

Accepted Manuscript

This article can be cited before page numbers have been issued, to do this please use: Y. Liu, B. Momani, H. H. Winter and S. L. Perry, *Soft Matter*, 2017, DOI: 10.1039/C7SM01285C.

ROYAL SOCIETY OF CHEMISTRY

rsc.li/soft-matter-journal

View Article Online
DOI: 10.1039/C7SM01285C

Journal Name

ARTICLE

Rheological Characterization of Liquid-to-Solid Transitions in Bulk Polyelectrolyte Complexes

Received 00th January 20xx,
Accepted 00th January 20xx

DOI: 10.1039/x0xx00000x

www.rsc.org/

Yalin Liu,[a] Brian Momani,[a] H. Henning Winter,[a] Sarah L. Perry*[a]

Polyelectrolyte complexation has long been known to result in both liquid and solid complexes. However, the exact nature of the liquid-to-solid transition remains an open question. We have used rheology to explain this phenomenon for the model system of poly(4-styrenesulfonic acid, sodium salt) (PSS) and poly(diallyldimethyl ammonium chloride) (PDADMAC) in the presence of potassium bromide (KBr). The use of a time-salt superposition allows for a detailed analysis of changes in the linear viscoelastic response for both liquid complex coacervates and solid polyelectrolyte complexes as a function of salt concentration, and facilitates unambiguous determination of the mechanism for this phase transition. Decreasing salt concentration, and the commensurate decrease in the water content of PSS/PDADMAC/KBr complexes is shown to lead to the formation of a physical gel due to the development of a network with trapped electrostatic crosslinks that percolates the sample at a critical salt concentration.

Introduction

Polyelectrolyte complexation is the result of electrostatic and entropically-driven interactions between oppositely charged polymers or macro-ions in water. The subsequent associative phase separation leads to the formation of a polymer-rich phase that can be either liquid or solid, in equilibrium with a polymer-poor supernatant.[1-9] Liquid-liquid phase separation is known as complex coacervation. The self-assembly of these highly-hydrated, polymer-rich coacervate phases can be controlled by the ratio of positive-to-negative charges in the system, the polymer chemistry and chain length, polymer charge density, ionic strength, pH, etc.[1-19] Coacervates are a class of materials that have a long history of use in the food and personal care industries, and are increasingly finding traction as a platform for drug and gene delivery, and as underwater adhesives.[3,6-10,14,18,19] In contrast, solid polyelectrolyte complexes have found little utility due to their resistance to traditional thermal- or solvent-based processing methods.

While both complex coacervation and solid precipitation have been reported for a wide variety of systems, little is known about the mechanistic interactions that dictate the formation of liquid vs. solid complexes.[1,7,14,16,18,20,21] Recently, Schlenoff *et al*. demonstrated the use of salt as a plasticizing agent to enable the continuous transformation of bulk solid polyelectrolyte complexes into liquid coacervates, and ultimately a single-phase solution.[11,16,21,22] Similar efforts on layer-by-layer films have demonstrated the importance of both salt and water on the mechanical properties of the resulting materials.[3,7-9,23,24] However, the mechanism driving this observed liquid-to-solid transition has yet to be determined, and as such, identification of a critical transition state can be challenging.

Here, we make use of small amplitude oscillatory shear linear viscoelastic measurements to enable a general, frequency independent characterization of the liquid-to-solid transition observed in polyelectrolyte complexes as a function of salt concentration. The point at which a liquid transitions to a solid can be identified from frequency sweep data. For chemical and physical gels, the relaxation modulus $G(t)$ is known to adopt a power-law format at the gel point of the form:

$$G(t) = G_0\left(\frac{t}{\tau_0}\right)^{-n} \quad (1)$$

where $0 < n < 1$ and G_0 is related to the stiffness of the critical gel.[1] As a consequence of this power-law relaxation, several linear viscoelastic material functions become frequency invariant, such as $\tan(\delta)$, $2\delta/\pi$, G'/G^*, G''/G^* and the front factor $G_0\tau_0^n$. In contrast, a glass transition is typically identified by the divergence of the characteristic time associated with long-range connectivity in the sample (*i.e.*, a diverging α transition), which results in a relaxation modulus[12,25,26] with

$$G(t) = H_\alpha \int_o^{\tau_{\max}} \frac{d\tau}{\tau}\left(\frac{\tau}{\tau_{\max}}\right)^m e^{-t/\tau} \quad (2)$$

[a] Department of Chemical Engineering, University of Massachusetts Amherst, Amherst, MA 01003, USA. Electronic mail: perrys@engin.umass.edu

Electronic Supplementary Information (ESI) available: Materials characterization, sample preparation, turbidity data and detailed rheology data. See DOI: 10.1039/x0xx00000x

View Article Online
DOI: 10.1039/C7SM01285C

$0 < m < 1$ and a diverging longest relaxation time τ_{max} in the approach of the glass transition. Once this point of transition has been identified, the stress relaxation behaviour, or relaxation time spectra, for samples on both sides of the transition can be examined to confirm the nature of the transition (*i.e.*, as gelation, or a glass transition) and allow for further characterization of the material.[3,6-10,14,18,19] However, one challenge in applying this approach is the limited range of frequency space over which linear viscoelastic measurements can be performed on a single sample. To overcome this limitation, Spruijt *et al*. used time-salt superposition in conjunction with a sticky Rouse model to describe the salt-driven superposition of linear viscoelastic data for various coacervate samples.[6,12,14,16,18-20] We also take advantage of a time-salt superposition strategy but do not restrict the superposition to a specific model.

Materials and Methods

Polymer Characterization

Poly(4-styrenesulfonic acid, sodium salt) (PSS) was purchased as a 15 wt% solution in water (AkzoNobel, VERSA TL130). Poly(diallyldimethylammonium chloride) (PDADMAC) was purchased as a 20 wt% solution in water (average M_w 200,000-350,000 medium molecular weight, Sigma-Aldrich). Both polymers were characterized by gel permeation chromatography (GPC Agilent Technologies, TSKgel 3000). GPC of PDADMAC was performed using a volume ratio 50/50 mixture of 0.5M sodium acetate ($C_2H_3NaO_2$, ACS Grade, Fisher) and 0.5M acetic acid (CH_3COOH, ACS Grade, Fisher) as the mobile phase. PSS was tested using a volume ratio 80/20 mixture of 0.1M sodium nitrate ($NaNO_3$, Sigma-Aldrich) and acetonitrile (C_2H_3N, ACS Grade, Fisher). The PDADMAC sample was prepared in mobile phase at a concentration of 2.1 mg/mL while PSS sample was prepared in mobile phase at 2.2 mg/mL. The flow rate was 1 mg/mL for both samples. Assuming 100% mass recovery, analysis of molecular weight based on multi-angle light scattering (Wyatt Technology, DAWN HELEOS II) determined that PSS has an average molecular weight M_w~ 354,400 g/mol with a polydispersity index (PDI = M_w/M_n) of 1.7, while PDADMAC has an average M_w~289,100 g/mol and an apparent PDI of 1.3.

Sample Preparation

Stock solutions of 0.125M (on a monomer basis) were prepared via dilution with Milli-Q water (resistivity of 18.2 MΩ cm, Millipore, USA) and filtered through a 0.22 μm filter (poly(ethersulfone), Thermo Scientific). Stock solutions of 4M KBr (ACS Grade, Fisher) and 2.5M KBr were prepared gravimetrically. To make coacervates, water, followed by KBr solution, 0.125M PSS, and 0.125M PDADMAC were added into a 50 mL Falcon tube. Samples were vortexed after each addition to ensure complete mixing. Following preparation, samples were examined using an optical microscope (EVOS FL Auto). Samples were then centrifuged at 4,000 rpm (Thermo Scientific Legend R1X) for five minutes to coalescence the dense phase, and stored overnight at room temperature (~25°C) to allow for sample equilibration. Additional details are available in the Supporting Information.

Rheometry

Experiments were performed using a Malvern Kinexus Pro stress-controlled instrument, run in strain-controlled oscillatory mode. A 20 mm diameter stainless steel parallel plate fixture with a solvent trap was utilized for all rheological experiments for salt concentrations between 0.5M and 1.5M. For salt concentrations above 1.5M, a 50 mm 2° cone-and-plate fixture was used. Experiments were run at 25°C. The strain amplitude used in the measurements was between 0.1% to 1%. This strain was confirmed to be in the linear viscoelastic region for all samples by strain-sweep experiments. The rheological data were salt-shifted, and their relaxation time spectrum was calculated using the IRIS software package.[11,16,21,22] Additional details are available in the Supporting Information.

Turbidimetry

Turbidity was used to qualitatively measure of the extent of coacervation as a function of charge stoichiometry and salt concentration. Turbidity measurements were made at 562 nm using a microplate reader (BioTek Synergy H1). Samples were prepared using the same protocol as for rheology samples but at a 200-μL scale and were not centrifuged. After preparation, 50 μL of sample was pipetted in triplicate into a 384-well plate (Fisher) for analysis. Each sample was measured in triplicate. Turbidity data are available in the Supporting Information (Figs. S1,2).

Phase Diagram Determination

Samples for phase diagram determination (*i.e.*, quantification of the concentration of polymer and salt in both the coacervate phase and the supernatant phase) were prepared as above and analysed using a method described previously.[3,7-9,23] Briefly, following centrifugation, the volume of the supernatant was determined by decanting into a volumetric cylinder. The volume of the coacervate phase was calculated as the difference between the measured supernatant volume and the total preparative volume of 50 mL, typically in the range of 1-2 mL. The concentrations of salt and polymer in the supernatant phase were measured directly. These values, along with the volumes of the coacervate and supernatant phases were then used to calculate the concentration of salt and polymer in the coacervate phase. The concentration of salt in the supernatant phase was measured via conductivity (TetraCon 325). Each sample was measured three times, and averaged. Conversion to concentration was then performed using calibration curves generated from a set of standard samples. The concentration of PSS in the supernatant phase was measured via UV/Vis spectroscopy (BioTek Take 3). Four samples of 3 μL each were placed on the microplate. The absorbance was then measured at a wavelength of 262 nm, corresponding to the peak absorbance of PSS. Conversion to

View Article Online
DOI: 10.1039/C7SM01285C

Journal Name

ARTICLE

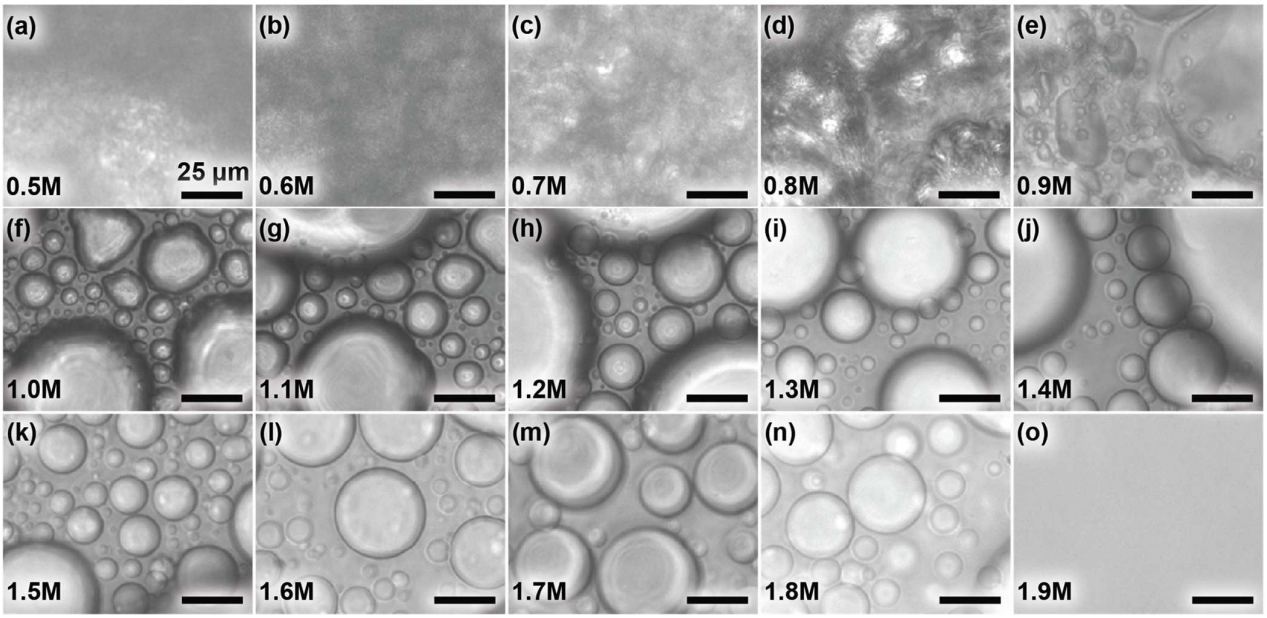

Fig 1. Optical micrographs of solid precipitates **(a-e)**, liquid complex coacervate droplets **(e-n)**, and a single-phase solution **(o)** resulting from the complexation of PSS and PDADMAC at increasing concentrations of KBr and 45 mM total initial monomer.

concentration was then performed using calibration curves generated from a set of standard samples. Our calculations assume that the concentration of PDADMAC present in the supernatant correlates directly with the measured value for PSS, which is reasonable as all samples were prepared using stoichiometric quantities of the two polymers. The measured concentration of polymer was then used to calculate the contribution of the polymers to the solution conductivity, which was then subtracted from the measured total. Finally, this polymer-corrected conductivity value was converted to a salt concentration using a calibration curve.

Results and Discussion

Here, we chose to work with the canonical saloplastic system of poly(4-styrenesulfonic acid, sodium salt) (PSS), poly(diallyldimethylammonium chloride) (PDADMAC), and potassium bromide (KBr).[4,8,27,28] Turbidity was used to confirm both the stoichiometry of interaction between the two polymers and to estimate the range of salt concentrations over which apparent precipitation (0 to 0.9M KBr) and coacervation (0.9M to 1.8M KBr) occur (Figs. S1 and S2 in the Supporting Information). Optical microscopy allowed for visual confirmation of the observed transitions from solid polyelectrolyte complexes (Fig. 1a-d), to liquid complex coacervates (Fig. 1e-n), and finally a single solution phase (Fig. 1o), with increasing salt concentration.

The initial dispersions of precipitates or coacervate droplets that formed upon mixing of PSS and PDADMAC (Fig. 1) were coalesced via centrifugation and isolated from the supernatant phase for subsequent characterization. Salt and polymer concentration were quantified for both the polymer-rich coacervate and the polymer-poor supernatant phase, allowing for plotting of the binodal phase boundary. As indicated in Fig. 2, we observed a 100-1000x increase in the concentration of polymer in the coacervate phase (plotted values are on a monomer basis), relative to the initial sample. Furthermore, our data clearly showed a strong partitioning of salt out of the coacervate phase, in agreement with recent theoretical and simulation results.[23,29] These data allow for direct correlation of the linear viscoelastic response of coacervate materials with respect to their actual composition, rather than the concentration at which the overall samples were prepared.

Analysis of frequency sweep data shows an increase in the overall magnitude of the storage (G') and loss (G'') moduli with decreasing salt concentration (Figs. 3a and S3), typical of sample stiffening. Furthermore, for liquid coacervate samples at high salt concentrations, the linear viscoelastic response

View Article Online
DOI: 10.1039/C7SM01285C

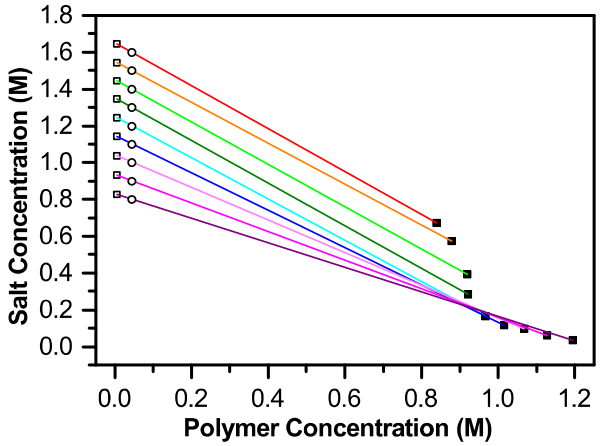

Fig. 2. Coacervate binodal curve as a function of polymer concentration and salt concentration. Open circles indicate the "as prepared" concentration of the overall samples. Coloured tie lines connect these initial conditions with the experimentally measured concentrations for the polymer-poor supernatant phase (open squares) and the polymer-rich coacervate phase (solid squares). The concentration of polymer is expressed on a monomer basis.

was dominated by the loss modulus. With decreasing salt concentration, one or more frequency-dependent crossovers between the storage and loss moduli can be observed. At the lowest salt concentrations, the viscoelastic response was dominated by the storage modulus over the entire frequency range, demonstrating the more solid-like character of the materials.

Figs. 3b and S4 show trends that are suggestive of a gelation-type transition. We observe decreasing values of $\tan(\delta)$ with increasing frequency for liquid-like samples at high salt concentration. The opposite behaviour is observed at the lowest salt concentrations, while a horizontal, frequency-invariant response is observed for intermediate salt concentrations near 0.8M to 1.0M KBr. Physically speaking, the condition where the elastic and viscous response of the material is independent of frequency, defines the liquid-to-solid transition. While this transition is most commonly looked for in a plot of $\tan(\delta)$ vs. frequency (Fig. 3b and S4), it can be challenging to unambiguously identify the transition point from a traditional plot of $\tan(\delta)$ vs. frequency for materials that do not show a strong elastic response in the solid state.

Replotting the data from Fig. 3 as a function of salt concentration, rather than frequency provides a simple and robust alternative method for visualizing the point of a material transition (Fig. 4). The plot of $\tan(\delta)$ vs. salt concentration (Fig. 4a) shows similar trends to those in Figs. 3b and S4. A relatively small increase in the loss tangent is observed at the low salt concentrations corresponding to solid samples, while a larger spread in the data is observed at high salt concentrations for liquid samples. However, a crossover point, corresponding to the frequency-invariant solid-to-liquid transition can be clearly identified at 0.85M KBr, despite the absence of direct data at that condition. In addition to using the traditional metric of tan(δ), related graphs of $2\delta/\pi$, G'/G^*, or G''/G^* vs. salt concentration provide additional perspectives on the viscoelastic response of the material. Plotting the normalized phase angle ($2\delta/\pi$) directly, rather than as the tangent of the phase angle (Fig. 4b) allows for a broader visual spread of the data at both high and low salt concentrations. Furthermore, this approach allows for direct determination of the power-law exponent for the resulting gel ($n = 2\delta/\pi$ at the transition). Thus, for our materials we observe $n = 0.35$, indicating a relatively stiff gel. Alternatively, the graphs of G'/G^* and G''/G^* are normalized graphs of $\cos(\delta)$ and $\sin(\delta)$, respectively, highlighting the relative contribution of the storage or loss modulus to the complex modulus (G^*). The data in Fig. 4c demonstrate that contribution of the storage modulus to the material response was more sensitive to frequency changes at high salt concentration, where it contributes the least to the overall complex modulus, while the opposite trends are observed for the relative impact of the loss modulus (Fig. 4d). However, it is important to note that the location of the crossover point, identifying the solid-to-liquid transition is invariant across all of these depictions at 0.85M KBr.

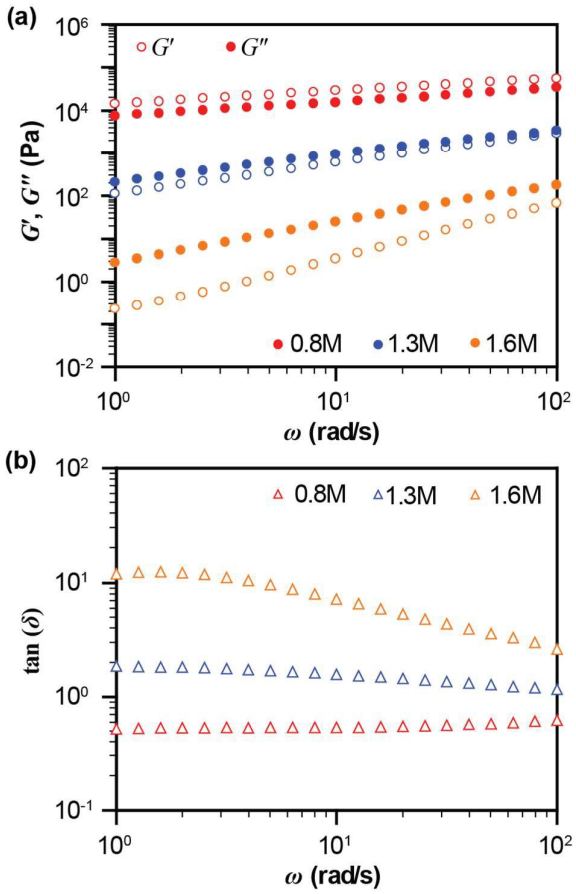

Fig. 3. Frequency sweep data for samples prepared at 0.8M (red), 1.3M (blue), and 1.6M (orange) KBr, shown as **(a)** the elastic modulus (G') and viscous modulus (G'') vs. frequency (ω), and as **(b)** the tangent of the phase angle (δ) vs. frequency (ω). Data for additional salt concentrations are available in the Supporting Information.

View Article Online
DOI: 10.1039/C7SM01285C

Journal Name

ARTICLE

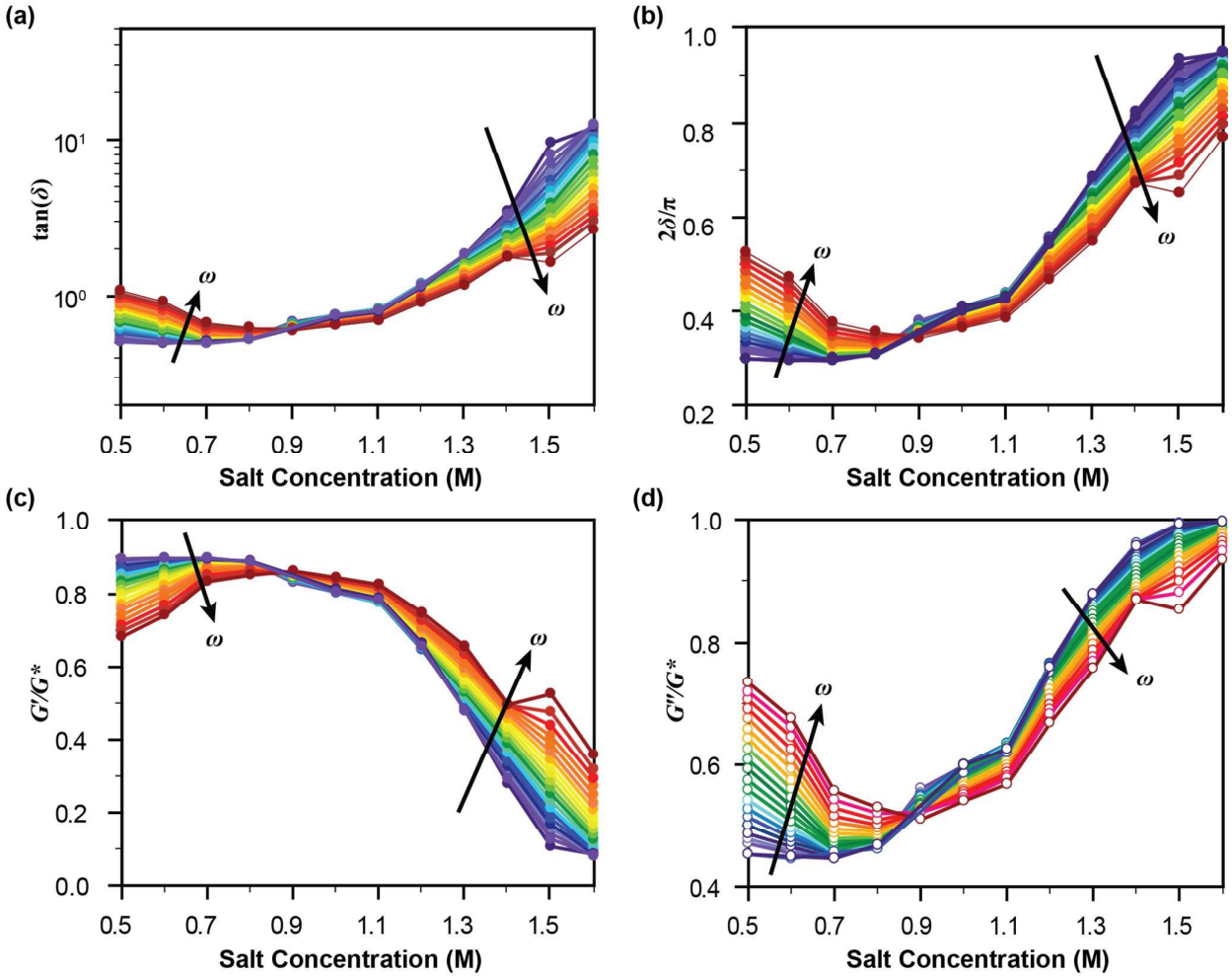

Fig 4. Plots of **(a)** $\tan(\delta)$, **(b)** the normalized phase angle ($2\delta/\pi$), **(c)** the normalized elastic modulus (G'/G^*), and **(d)** the normalized viscous modulus (G''/G^*) as a function of the "as prepared" salt concentration. Data are shown for oscillation frequencies ranging from 1 rad/s to 100 rad/s (purple to red), also indicated by the arrows. The gel point occurs at a salt concentration of 0.85M KBr and $2\delta/\pi = 0.35$, based on the location of the frequency-invariant crossover point visible in all figures.

Having identified the transition point, we then performed a time-salt superposition for both the liquid (Fig. 5a) and solid samples (Fig. 6a).[16,20,30,31] Solid samples in the range of 0.5M to 0.8M KBr were shifted relative to the "as prepared" 0.5M salt concentration, corresponding to the high frequency end of the plot. Similarly, liquid coacervate samples in the range of 1.0M to 1.6M KBr were shifted relative to the 1.0M "as prepared" sample. The dataset obtained at 0.9M KBr, very close to the solid-to-liquid transition, was excluded from this superposition because the sample response at the transition point was not continuous with either the liquid or solid sample. The resulting superposition allows for extension of the range of timescales over which the viscoelastic response is measured from only two decades in frequency space to three for solid samples, and nearly ten decades for liquid samples.

One seemingly obvious question would be why the superposition was not performed continuously over the entire range of liquid and solid samples. Less intuitively, the solid and liquid curves do not superimpose across the transition due to a lack of self-similarity between the liquid and solid materials that arises as a divergence in the relaxation behaviour of the sample at the gel point. In the approach to the critical gel point, the relaxation time of the liquid coacervate samples is dominated by the largest network of crosslinked polymers. At

View Article Online
DOI: 10.1039/C7SM01285C

Journal Name

ARTICLE

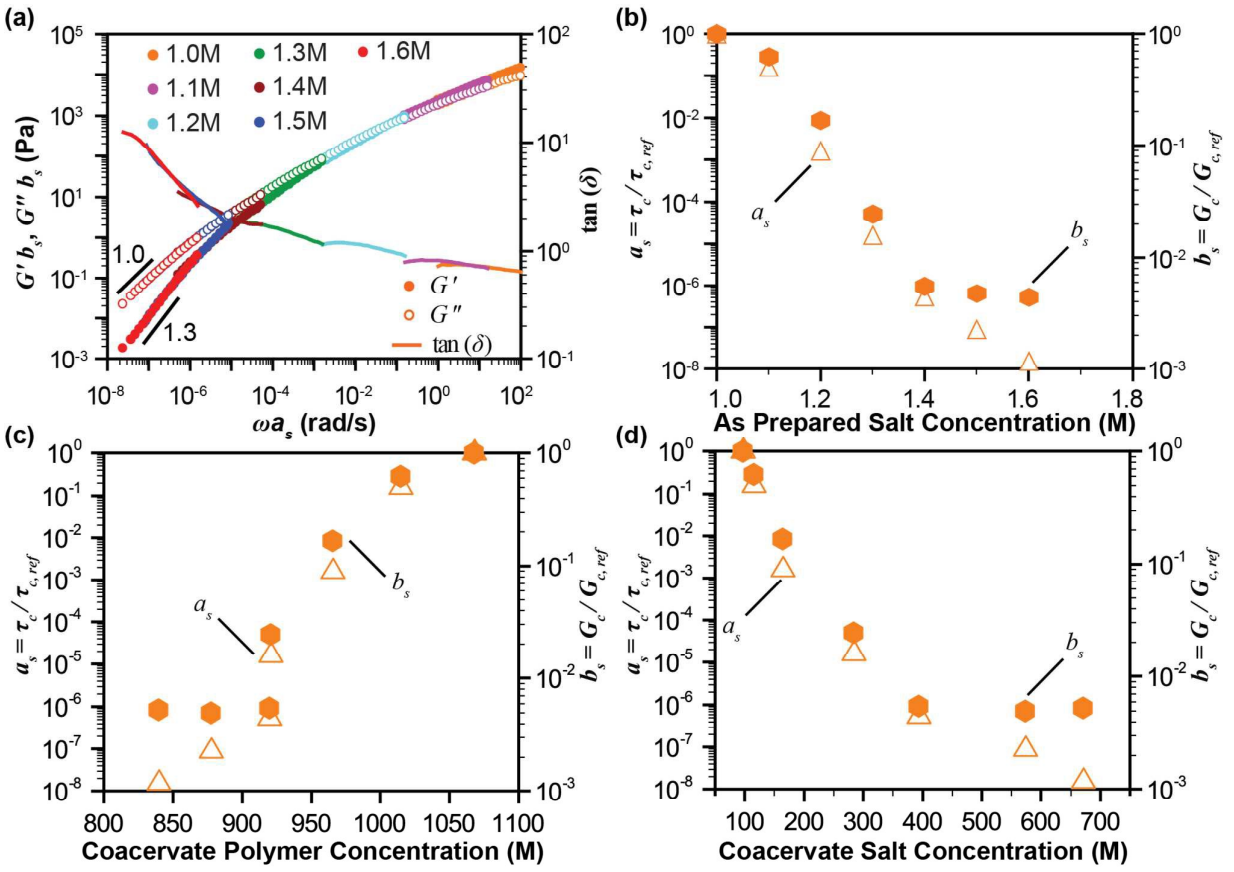

Fig. 5. (a) Plot of the time-salt superposition of frequency sweep data for liquid complex coacervates (1.0M to 1.6M KBr), shifted with respect to the 1.0M "as prepared" data. Legends indicate the "as prepared" salt concentration. Plot of the horizontal (open triangles) and vertical (solid hexagons) shift factors, a_s and b_s, for as a function of the **(b)** "as prepared" salt concentration. The same shift factors plotted with respect to the **(c)** measured polymer concentration (on a monomer basis) and **(c)** the measured salt concentration in the coacervate phase.

the transition point this crosslinked network percolates the sample and the relaxation time becomes infinite. Beyond the gel point, the relaxation behaviour of the sample is characterized by the remaining uncrosslinked domains.

The resulting superposition data for liquid-like samples (Fig. 5a) shows strong similarities to the rheological response of a polymer melt. At low frequency, the data suggest an approach to the terminal region, with the slope of the loss modulus (G") equalling the expected 1.0, but that for the storage modulus (G') only reaching 1.3, instead of the expected 2.0. At higher frequencies, a crossover is observed between the storage and loss moduli. However, we did not observe strong evidence of an entanglement plateau. In contrast, for the solid samples (Fig. 6a), the data at low frequency show parallel trends in both G' and G" with a slope of 0.3, potentially reminiscent of a rubbery plateau, followed by another crossover point at high frequency. While the presence of such crossover points between the storage and loss moduli have been used previously as a means for defining a liquid-to-solid transition, it is important to note that such crossover points are inherently frequency dependent.[4,11,13-17,32] In contrast, here we have described a more universal, frequency invariant approach to more accurately define such transitions.

Time-salt superposition requires both a horizontal and a vertical shift to account for salt-induced changes in the stress-relaxation behaviour of the material. The corresponding horizontal and vertical shift factors (a_s and b_s) are shown as a function of the "as prepared" salt concentration in Figs. 5b and 6b for the liquid and solid samples, respectively. The vertical

View Article Online
DOI: 10.1039/C7SM01285C

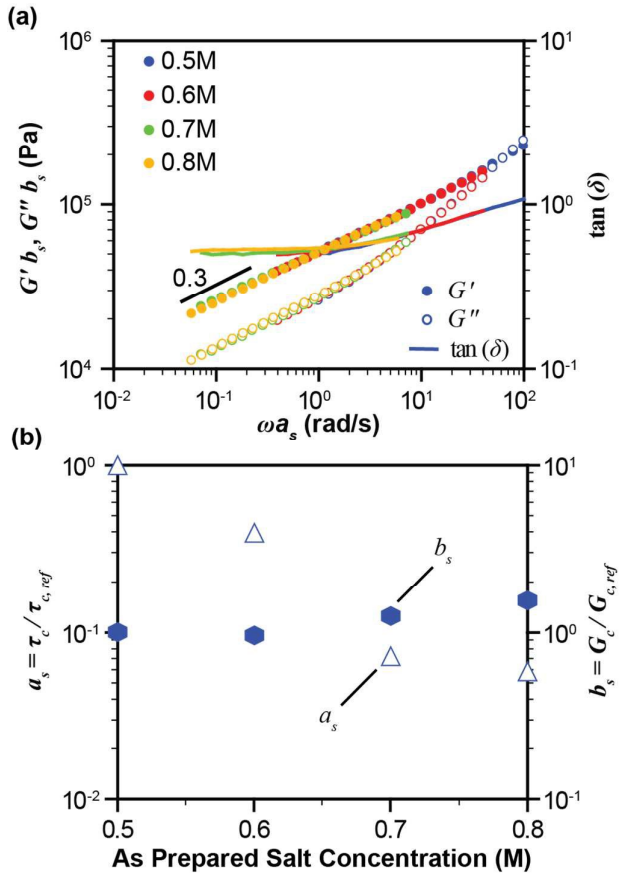

Fig. 6. (a) Plot of the time-salt superposition of frequency sweep data for solid polyelectrolyte complex samples (0.5M to 0.8M KBr), shifted with respect to the 0.5M "as prepared" data. **(b)** Plot of the horizontal (open triangles) and vertical (solid hexagons) shift factors, a_s and b_s, as a function of the "as prepared" salt concentration.

shift factor (b_s) serves as a correction to the moduli to account for differences in polymer concentration at the different salt concentrations. For solid samples, a small increase in the magnitude of the vertical shift factor was observed with increasing salt concentration (Fig. 6b). However, for coacervate samples in the liquid state, the vertical shift factor decreases sharply, almost exponentially, for "as prepared" salt concentrations of 1.0M to 1.4M KBr, followed by very little change up to 1.6M KBr (Fig. 5b), with similar trends observed for the measured salt concentrations over the range of 100 mM to 700 mM KBr (Fig. 5d). It is unclear why the vertical shift factors show opposite trends as a function of salt concentration for liquid and solid samples.

As expected from the data in Fig. 2, the concentration of polymer present in liquid complex coacervates decreases with increasing salt concentration. Thus, we observe a trend of increasing vertical shift factor with increasing polymer concentration (Fig. 5c). We would have expected similar trends for solid materials;[33] however, direct measurements of the polymer concentration present in solid samples is much more challenging than for liquid samples, and beyond the scope of the current work. Thus, while variations in salt and polymer concentration may account for the differences in the observed shift factors, further investigations are needed to clarify the physical origins of this observation. It is also interesting to note that the dramatic trends in the vertical shift factor for the liquid coacervate samples in our PSS/PDADMAC/KBr system were much more significant than has been reported previously for other coacervate systems.[14,16] However, it is unclear whether this is a characteristic of the polymer systems chosen, or is a consequence of the ability of this particular polymer system to undergo a liquid-to-solid transition.

The horizontal shift factor (a_s), accounts for changes in the stress-relaxation behaviour of the material. Previously, such behaviour in coacervates has been described using a sticky Rouse model, where the "sticky" friction between chains is the electrostatic interactions driving the self-assembly of the material.[16,19,21,34] The timescale for shifting these materials can be related to the activation energy barrier for the rearrangement of two ion pairs, which is related to the salt concentration. Thus, increasing salt concentration can be seen as effectively decreasing the friction for motion of the polymer chains. Both liquid and solid samples showed an exponential-like decrease in the horizontal shift factor as a function of salt concentration (Figs. 5 and 6), similar to the trends observed in previous reports.[16,19,35] However, the magnitude of the shift was significantly lower for solid samples than for liquid. Based on the relationship between salt and polymer concentration in the coacervate phase, an exponential-like trend of increasing shift factor with increasing polymer concentration was also seen for the liquid samples (Fig. 5c). Additionally, the slope of the observed shift factors for the liquid samples was more strongly negative for the PSS/PDADMAC/KBr system, than has been reported for other polymer systems previously.[14,16,35]

In the same way that time-salt superposition allows us to more broadly characterize the frequency response of our materials, we were able to use these shifted data to further confirm the liquid-to-solid transition occurring within our samples. Fig. 7a shows a plot of complex viscosity (η^*) as a function of complex modulus (G^*). This so-called Winter plot clearly highlights a divergence in the material response for the solid and liquid samples at the critical gel point.[10,36,37] The transition can be calculated based on the power-law exponent determined from Fig. 4 ($n = 0.35$). The transition visualized as the divergence line in the Winter plot, and is expected to have a slope of $(n-1)/n$, or –1.9, which matches well with our data.

Additional analysis of the relaxation behaviour of our materials further highlights the consistency of our data with the expected behaviour of a physical gel. A plot of the relaxation time spectra (H) for the liquid coacervate samples shows the characteristic decay in the relaxation modes to zero at sufficiently long times (Fig. 7b). While a glass transition would have been characterized by shifting of this liquid-like relaxation behaviour to longer times, we instead observe the suggestion of a plateau in the relaxation spectrum for the solid samples, supportive of gelation as the physical mechanism for the transition.[10,20,38,39]

The divergence in this relaxation behaviour again highlights why it is aphysical to perform a time-salt superposition to

View Article Online
DOI: 10.1039/C7SM01285C

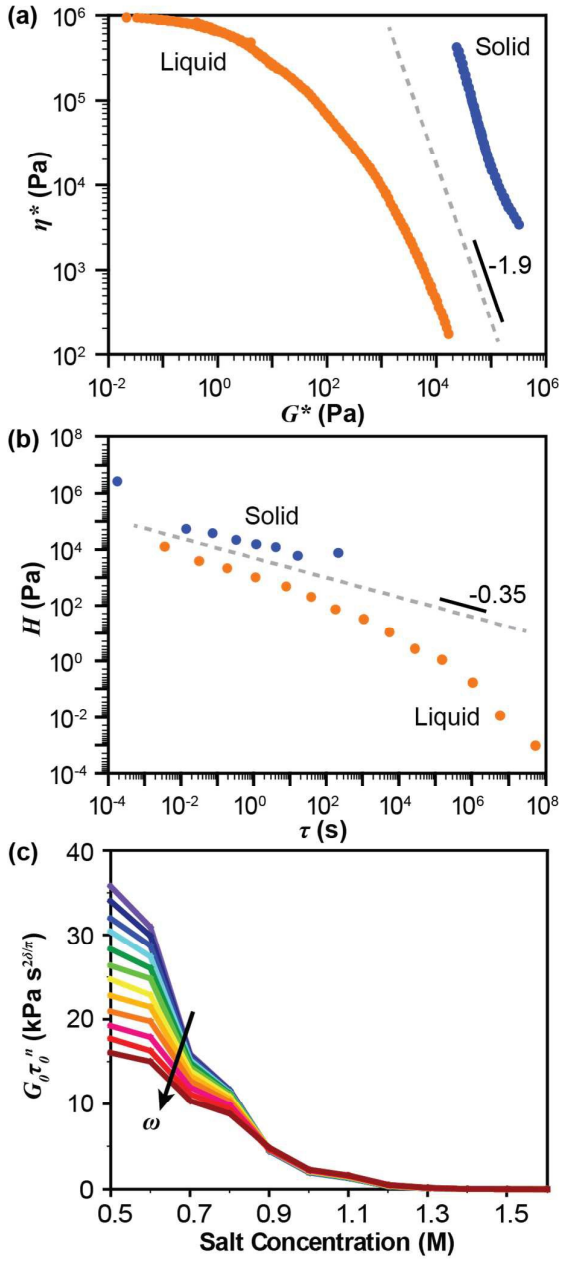

Fig. 7. (a) A plot of complex viscosity (η^*) as a function of complex modulus (G^*) for liquid (orange, 1.0M to 1.6M KBr) and solid (blue, 0.5M to 0.8M KBr) "as prepared" data resulting from the time-salt shifted frequency sweep data shown in Fig. 4. The dashed grey line with slope of 1.9 indicates the predicted divergence line with the expected power-law behaviour at the gel point. The divergence between the two data sets indicates a solid-to-liquid transition in the range of 0.8M to 1.0M KBr. **(b)** A plot of the relaxation time spectrum (H) as a function of relaxation time (τ) for data from **(a)**, showing the characteristic decrease in the relaxation time spectrum at long times for liquids (orange) and suggesting a gel-like plateau in the relaxation time spectrum for solid samples (blue). The dashed grey line with slope of 0.35 indicates the expected power-law relaxation behaviour of the material at the gel point. **(c)** A plot of the front factor $G_0\tau_0^n$ as a function of KBr salt concentration. Data are shown for oscillation frequencies ranging from 66.7 rad/s to 100 rad/s (purple to red).

combine data for both liquid and solid samples onto a single curve. As the liquid samples approach the critical gel point, the relaxation behaviour of the sample is dominated by the relaxation time of the largest crosslinked network in the sample. The critical gel point occurs when these crosslinks create a percolated network that spans the sample. At this point, the percolated gel is trapped and can no longer relax, resulting in the observed divergence in the relaxation time spectrum. For solid samples beyond the critical gel point, the timescales for relaxation are dominated by smaller clusters of molecules that are not integrated into the percolated network, and decrease with increasing crosslink density.

The description of the observed salt-driven, solid-to-liquid transition is consistent with the utility of the sticky Rouse model, where "sticky" electrostatic interactions between chains act as friction points that modulate the stress relaxation behaviour of the material as a function of salt concentration. Fig. 8 provides a visual depiction of the proposed gelation mechanism driving the liquid-to-solid transition observed in these polyelectrolyte complex materials. The self-assembly of the material is driven by the electrostatic and entropic interactions between oppositely-charged polymers. At high concentrations of salt, sufficient salt ions and water are available to provide extrinsic charge compensation for charged groups along the polymer chains that are not engaged in direct electrostatic interactions with another polymer.[30,33] These types of extrinsic charge pairs facilitate chain rearrangement, lowering the activation energy barrier, or the friction for such motions.[40] However, as the concentration of salt in the system is lowered, fewer ions are available to facilitate chain motion, increasing the apparent friction of the interaction. As further salt is removed from the system, ion pairs between polymers become trapped and unable to rearrange, excluding water. Gelation occurs when the network of these trapped crosslinks percolate the sample. It should be noted that salt-driven transitions have been reported previously for PSS/PDADMAC/KBr, and have been attributed to a glass transition-like mechanism based on results from dynamic mechanical testing and differential scanning calorimetry.[3,7,8,10,30,41] While the previous experiments were performed over a different range of salt conditions and using polymers with different molecular weights, it is intriguing to speculate whether these two phenomena are related, or represent distinct salt-driven transitions in saloplastic materials.

To complete the theoretical description of the observed gelation phenomenon, the frequency-invariant front factor $G_0\tau_0^n$ can be determined using a strategy similar to that presented in Fig. 4. Fig. 7c shows a plot of $G_0\tau_0^n$ vs. salt concentration. From this plot, the value of $G_0\tau_0^n = 6600$ Pa s can be read for the transition point of 0.85M KBr. This type of plot can be generated from the storage modulus G', loss modulus G", or complex modulus G*, using the relationships shown in Eqs. (3) ¬ (5) below, where Γ is the gamma function.

$$G'(\omega) = \frac{\pi G_0}{2\Gamma(n)\sin(n\pi/2)}\frac{(\omega\tau_0)^n}{} \qquad (3)$$

View Article Online
DOI: 10.1039/C7SM01285C

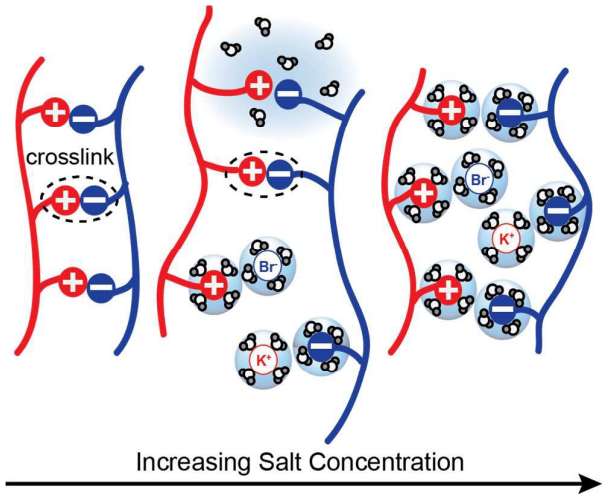

Fig. 8. Schematic depiction of the salt-induced gelation observed in polyelectrolyte complexes. Decreasing salt, and thus water concentration results in the formation of trapped ion pair interactions that can ultimately percolate the sample and lead to gelation.

$$G''(\omega) = \frac{\pi G_0}{2\Gamma(n)\cos(n\pi/2)} \frac{\left(\omega\tau_0\right)^n}{} \quad (4)$$

$$G^*(\omega) = \frac{\pi G_0}{2\Gamma(n)\sin(n\pi/2)\cos(n\pi/2)} \frac{\left(\omega\tau_0\right)^n}{} \quad (5)$$

The values of $G_0\tau_0^n = 6{,}600$ Pa s and $n = 0.35$ indicate a relatively stiff gel that has relatively long relaxation time as it approaches gel point.

Conclusions

We have unambiguously identified the salt-driven liquid-to-solid transition in the polyelectrolyte complex system of PSS/PDADMAC/KBr system as gelation, using a frequency-invariant analysis strategy of time-salt superposition data obtained via small amplitude oscillatory shear.[42] To the best of our knowledge, this is the first report to investigate the dynamic mechanical response of polyelectrolyte complexes in both the liquid coacervate and the solid state, and to identify the transition dynamics. While the overall trends are qualitatively consistent with previous reports focused on characterizing the rheological response of liquid coacervates, we observed quantitative differences that could be a consequence of the different polymers used in this study, the saloplastic nature of this system, or both. For instance, the polymers used in this study are relatively more hydrophobic than those used by Spruijt *et al*.[16,35] Similarly, recent reports on polypeptide-based complex coacervates highlighted the potential for hydrogen-bond driven precipitation.[11,43,44] It would be reasonable to assume that secondary interactions such as hydrogen bonding, hydrophobic interactions, pi-pi stacking, or even the interaction of the specific polymers with water could alter the scaling observed in the time-salt superposition. Further work, including a systematic study of how parameters such as polymer chemistry and structure, polymer chain length, charge stoichiometry, salt, pH, and other control parameters affect the stress-relaxation, and thus time-salt superposition behaviour, as well as the potential for saloplastic liquid-to-solid transitions is needed to create a more universal understanding of this class of materials.

Acknowledgements

Acknowledgment is made to the Donors of the American Chemical Society Petroleum Research Fund for support of this research.

References

1 H. H. Winter and M. Mours, *Rheology of polymers near their liquid-solid transitions*, Adv. Polym. Sci, 1997.
2 D. S. Hwang, J. H. Waite and M. Tirrell, *Biomaterials*, 2010, **31**, 1080–1084.
3 E. Yildirim, E. Yildirim, Y. Zhang, Y. Zhang, J. L. Lutkenhaus, J. L. Lutkenhaus, M. Sammalkorpi and M. Sammalkorpi, *ACS Macro Lett.*, 2015, **4**, 1017–1021.
4 Q. Wang and J. B. Schlenoff, *Macromolecules*, 2014, **47**, 3108–3116.
5 D. S. Hwang, H. Zeng, A. Srivastava, D. V. Krogstad, M. Tirrell, J. N. Israelachvili and J. H. Waite, *Soft Matter*, 2010, **6**, 3232.
6 F. Comert, A. J. Malanowski, F. Azarikia and P. L. Dubin, *Soft Matter*, 2016, **12**, 4154–4161.
7 A. Vidyasagar, C. Sung, K. Losensky and J. L. Lutkenhaus, *Macromolecules*, 2012, **45**, 9169–9176.
8 A. Vidyasagar, C. Sung, R. Gamble and J. L. Lutkenhaus, *ACS Nano*, 2012, **6**, 6174–6184.
9 L. Shao and J. L. Lutkenhaus, *Soft Matter*, 2010, **6**, 3363–3369.
10 H. H. Winter, *Macromolecules*, 2013, **46**, 2425–2432.
11 S. L. Perry, L. Leon, K. Q. Hoffmann, M. J. Kade, D. Priftis, K. A. Black, D. Wong, R. A. Klein, C. F. Pierce, K. O. Margossian, J. K. Whitmer, J. Qin, J. J. de Pablo and M. Tirrell, *Nature Communications*, 2015, **6**, 6052.
12 E. Spruijt, A. H. Westphal, J. W. Borst, M. A. Cohen Stuart and J. van der Gucht, *Macromolecules*, 2010, **43**, 6476–6484.
13 S. Perry, Y. Li, D. Priftis, L. Leon and M. Tirrell, *Polymers*, 2014, **6**, 1756–1772.
14 D. Priftis, K. Megley, N. Laugel and M. Tirrell, *J. Colloid Interface Sci.*, 2013, **398**, 39–50.
15 R. Chollakup, J. B. Beck, K. Dirnberger, M. Tirrell and C. D. Eisenbach, *Macromolecules*, 2013, **46**, 2376–2390.
16 E. Spruijt, *Macromolecules*, 2013, **46**, 1633–1641.
17 K. Kaibara, T. Okazaki, H. B. Bohidar and P. L. Dubin, *Biomacromolecules*, 2000, **1**, 100–107.
18 D. Priftis and M. Tirrell, *Soft Matter*, 2012, **8**, 9396–9405.
19 Y. Liu, H. H. Winter and S. L. Perry, *Adv. Colloid Interface Sci.*, 2017, **239**, 46–60.
20 E. Spruijt, J. Sprakel, M. Lemmers, M. A. C. Stuart and J. van der Gucht, *Phys. Rev. Lett.*, 2010, **105**, 208301.
21 E. Spruijt, *Macromolecules*, 2013, **46**, 4596–4605.
22 H. H. Winter and M. Mours, *Rheol Acta*, 2006, **45**, 331–338.
23 M. Radhakrishna, K. Basu, Y. Liu, R. Shamsi, S. L. Perry and C. E. Sing, *Macromolecules*, 2017, **50**, 3030–3037.
24 J. A. Jaber and J. B. Schlenoff, *J. Am. Chem. Soc.*, 2006, **128**, 2940–2947.
25 H. H. Winter, M. Siebenb rger, D. Hajnal, O. Henrich, M. Fuchs and M. Ballauff, *Rheol Acta*, 2009, **48**, 747–753.

View Article Online
DOI: 10.1039/C7SM01285C

26 M. Siebenbürger, M. Fuchs, H. Winter and M. Ballauff, *J. Rheol.*, 2009, **53**, 707–726.
27 C. H. Porcel, C. H. Porcel, J. B. Schlenoff and J. B. Schlenoff, *Biomacromolecules*, 2009, **10**, 2968–2975.
28 P. Schaaf and J. B. Schlenoff, *Adv. Mater.*, 2015, **27**, 2420–2432.
29 S. L. Perry and C. E. Sing, *Macromolecules*, 2015, **48**, 5040–5053.
30 R. F. Shamoun, R. F. Shamoun, H. H. Hariri, H. H. Hariri, R. A. Ghostine, R. A. Ghostine, J. B. Schlenoff and J. B. Schlenoff, *Macromolecules*, 2012, **45**, 9759–9767.
31 M. Tekaat, D. Bütergerds, M. Schönhoff, A. Fery and C. Cramer, *Phys. Chem. Chem. Phys.*, 2015, **17**, 22552–22556.
32 A. Momeni and M. J. Filiaggi, *J. Rheol.*, 2016, **60**, 25–34.
33 R. F. Shamoun, A. Reisch and J. B. Schlenoff, *Adv. Funct. Mater.*, 2012, **22**, 1923–1931.
34 R. H. Colby, *Rheol Acta*, 2009, **49**, 425–442.
35 E. Spruijt, J. Sprakel, M. A. Cohen Stuart and J. van der Gucht, *Soft Matter*, 2010, **6**, 172–178.
36 H. H. Winter and F. Chambon, *J. Rheol.*, 1986, **30**, 367–382.
37 H. H. Winter, *Rheol Acta*, 2009, **48**, 241–243.
38 J. T. Cirulis, F. W. Keeley and D. F. James, *J. Rheol.*, 2009, **53**, 1215–1228.
39 S. Lindhoud and M. A. C. Stuart, in *Advances in Polymer Science*, Springer Berlin Heidelberg, Berlin, Heidelberg, 2012, vol. 255, pp. 139–172.
40 R. Zhang, Y. Zhang, H. S. Antila, J. L. Lutkenhaus and M. Sammalkorpi, *J. Phys. Chem. B*, 2017, **121**, 322–333.
41 W. C. W. Chen, B. G. Lee, D. W. Park, K. Kim, H. Chu, K. Kim, J. Huard and Y. Wang, *Biomaterials*, 2015, **72**, 138–151.
42 C. W. Macosko, *Rheology: Principles, Measurements, and Applications*, VCH Publishers, 1st ed. 1994.
43 K. Q. Hoffmann, S. L. Perry, L. Leon, D. Priftis, M. Tirrell and J. J. de Pablo, *Soft Matter*, 2015, **11**, 1525–1538.
44 N. M. Pacalin, L. Leon and M. Tirrell, *Eur. Phys. J. Spec. Top.*, 2016, **225**, 1805–1815.

View Article Online
DOI: 10.1039/C7SM01285C

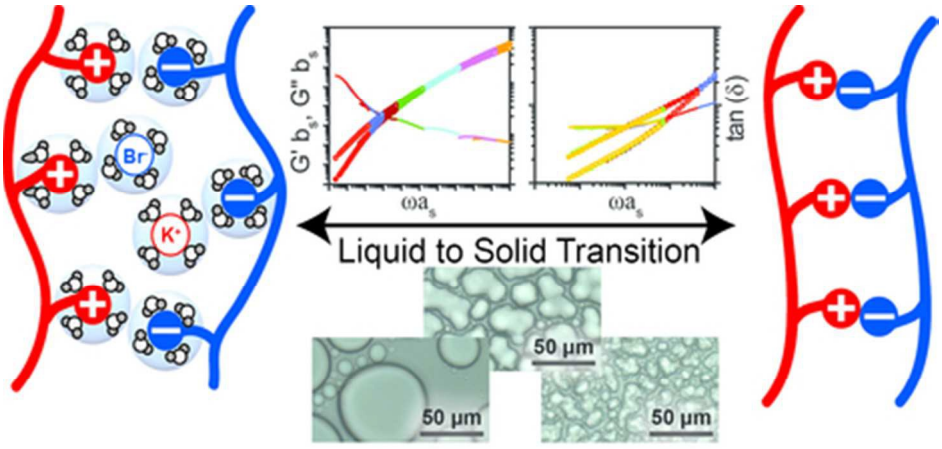

Table of Contents Figure

39x19mm (300 x 300 DPI)